

Is shrub expansion into grasslands pushed or pulled? A
spatial integral projection model for woody plant
encroachment

Trevor Drees^{*a,b}, Brad M. Ochocki^b, Scott L. Collins^c, and Tom E.X. Miller^b

^aDepartment of Biology, Penn State University, State College, PA USA

^bProgram in Ecology and Evolutionary Biology, Department of BioSciences, Rice
University, Houston, TX USA

^cDepartment of Biology, University of New Mexico, Albuquerque, NM USA

July 5, 2022

^{*}thd5066@psu.edu

1 Abstract

2 **Encroachment**¹ of shrubs into adjacent grasslands has become an increasingly reported
3 phenomenon across the world, and such encroachment is either pulled forward by high
4 population growth at the low-density encroachment front or pushed forward by higher-
5 density areas behind the front. However, at sites such as Sevilleta National Wildlife
6 Refuge in central New Mexico, little is known about whether encroachment is pushed or
7 pulled, and the dynamics of encroachment are not well-understood. Here, long-term en-
8 croachment of creosotebush (*Larrea tridentata*), a native perennial shrub, stands in stark
9 contrast with the stagnation in encroachment observed in recent decades. In order to
10 better understand creosotebush encroachment at this site, we quantify it using a spatially
11 structured population model where a wave of individuals travels at a speed governed by
12 both dispersal and density-dependence. Results indicate that population growth rates
13 generally increase with decreasing density, suggesting that encroachment is pulled by
14 individuals at the low-density wave front, and the spatial population model predicts an
15 encroachment rate of less than 2 cm per year. While the predicted rate of encroach-
16 ment is consistent with observations over recent decades, it does not explain long-term
17 creosotebush encroachment at the study site, suggesting that this process may occur in
18 pulses when recruitment, seedling survival, or dispersal significantly exceed typical rates.
19 Overall, our work demonstrates that individuals at low densities are likely the biggest
20 contributors to creosotebush encroachment at this site, and that this encroachment is
21 likely a process that occurs in large but infrequent bursts rather than at a steady pace.

22 Keywords

23 density-dependence, ecotones, woody encroachment, shrubs, integral projection model,
24 grassland

¹*I am not editing the abstract for now.*

25 Introduction

26 The recent and ongoing encroachment of shrubs and other woody plants into adjacent
27 grasslands has caused significant vegetation changes across arid and semi-arid landscapes
28 worldwide (Van Auken, 2000, 2009; Goslee et al., 2003; Gibbens et al., 2005; Parizek et al.,
29 2002; Cabral et al., 2003; Trollope et al., 1989; Roques et al., 2001). The process of en-
30 croachment generally involves increases in the number or density of woody plants in both
31 time and space (Van Auken, 2000), which can drive shifts in plant community structure
32 and alter ecosystem processes (Schlesinger et al., 1990; Ravi et al., 2009; Schlesinger
33 and Pilmanis, 1998; Knapp et al., 2008). Other effects of encroachment include changes
34 in ecosystem services (Reed et al., 2015; Kelleway et al., 2017), declines in biodiversity
35 (Ratajczak et al., 2012; Sirami and Monadjem, 2012; Brandt et al., 2013), and economic
36 losses in areas where the proliferation of shrubs adversely affects grazing land and pastoral
37 production (Mugasi et al., 2000; Oba et al., 2000).

38 Woody plant encroachment can be studied through the lens of spatial population
39 biology as a wave of individuals that may expand across space and over time (Kot et al.,
40 1996; Neubert and Caswell, 2000; Wang et al., 2002; Pan and Lin, 2012). Theory pre-
41 dicts that the speed of wave expansion depends on two processes: local demography and
42 dispersal of propagules. First, local demographic processes include recruitment, survival,
43 growth, and reproduction, which collectively determine the rate at which newly colonized
44 locations increase in density and produce new propagules. Second, colonization events
45 are driven by the spatial dispersal of propagules, which is commonly summarized as a
46 probability distribution of dispersal distance, or “dispersal kernel”. The speed at which
47 expansion waves move is highly dependent upon the shape of the dispersal kernel, espe-
48 cially long-distance dispersal events in the tail of the distribution (Skarpaas and Shea,
49 2007). Both demography and dispersal may depend on plant size, since larger plants
50 often have improved demographic performance and release seeds from greater heights,

51 leading to longer dispersal distances (Nathan et al., 2011). Accounting for population
52 structure, including size structure, may therefore be important for understanding and
53 predicting wave expansion dynamics (Neubert and Caswell, 2000).

54 Theory predicts that the nature of conspecific density dependence is another critical
55 feature of expansion dynamics but this is rarely studied in the context of woody plant
56 encroachment. Expansion waves typically correspond to gradients of conspecific density
57 – high in the back and low at the front – and demographic rates may be sensitive to
58 density due to intraspecific interactions like competition or facilitation. If the demo-
59 graphic effects of density are strictly negative due to competitive effects that increase
60 with density then demographic performance is maximized as density goes to zero, at the
61 leading edge of the wave. Under these conditions, the wave is “pulled” forward by indi-
62 viduals at the low-density vanguard (Kot et al., 1996), and targeting these individuals
63 and locations would be the most effective way to slow down or prevent encroachment
64 (cite?). However, woody encroachment systems often involve positive feedbacks whereby
65 shrub establishment modifies the environment in ways that facilitate further shrub re-
66 cruitment. For example, woody plants can modify their micro-climates in ways that
67 elevate nighttime minimum temperatures, promoting conspecific recruitment and sur-
68 vival for freeze-sensitive species (D’Odorico et al., 2010; Huang et al., 2020). Positive
69 density dependence (or Allee effects) causes demographic rates to be maximized at higher
70 densities behind the leading edge, which “push” the expansion forward, leading to qualita-
71 tively different expansion dynamics (Kot et al., 1996; Taylor and Hastings, 2005; Sullivan
72 et al., 2017; Lewis and Kareiva, 1993; Veit and Lewis, 1996; Keitt et al., 2001). Pushed
73 expansion waves generally have different shapes (steeper density gradients) and slower
74 speeds than pulled waves (Gandhi et al., 2016), and may require different strategies for
75 managing or decelerating expansion (check Taylor and Hastings ref). The potential for
76 positive feedbacks is well documented in woody encroachment systems but it remains un-
77 clear whether and how strongly these feedbacks decelerate shrub expansion and influence

78 strategies for management of woody encroachment.

79 In this study, we linked woody plant encroachment to ecological theory for invasion
80 waves, with the goals of understanding how seed dispersal and density-dependent demog-
81 raphy drive encroachment, and determining whether the encroachment wave is pushed or
82 pulled. Throughout the aridlands of the southwestern United States, shrub encroachment
83 into grasslands is well documented (D’Odorico et al., 2012) but little is known about the
84 dispersal and demographic processes that govern it. Our work focused on encroachment
85 of creosotebush (*Larrea tridentata*) in the northern Chihuahuan Desert. Expansion of
86 this species into grasslands over the past 150 years has been well documented, leading to
87 decreased cover of *Bouteloua eriopoda*, the dominant foundation species of Chihuahuan
88 desert grassland (Gardner, 1951; Buffington and Herbel, 1965; Gibbens et al., 2005).
89 As in many woody encroachment systems, creosotebush expansion generates ecotones
90 marking a transition from dense shrubland to open grassland, with a transition zone in
91 between where shrubs can often be found interspersed among grasses (Fig. 1).

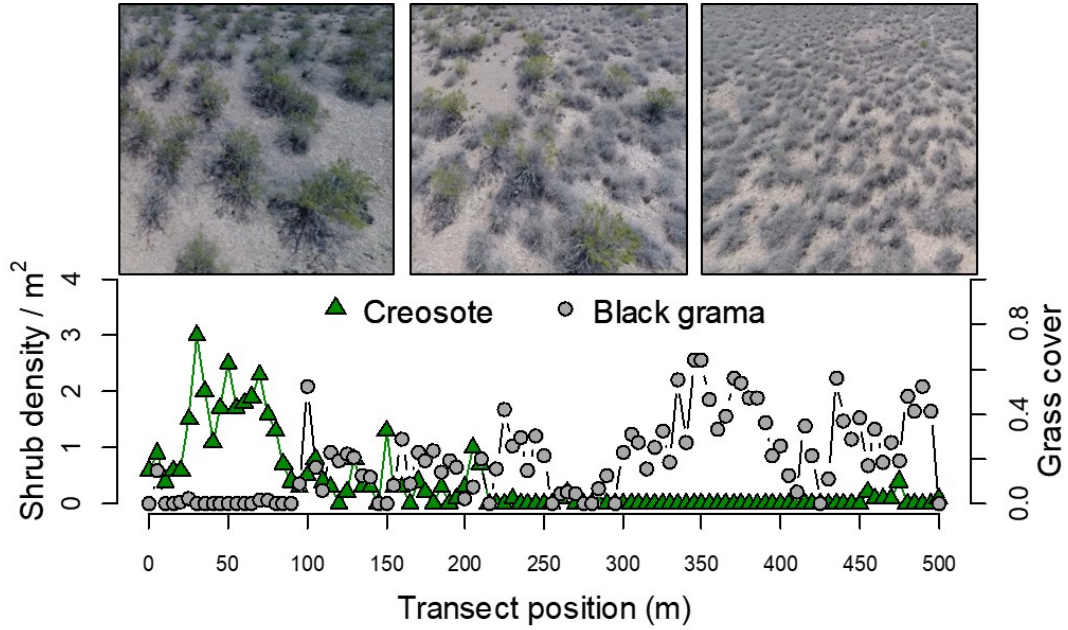


Figure 1: Example of an ecotone transect at Sevilleta LTER, spanning gradients of creosotebush and black grama grass. Photo credits: TEX Miller

Historically, creosotebush encroachment into grasslands is believed to have been driven by a combination of factors including overgrazing, drought, variability in rainfall, and suppression of fire regimes Moreno-de las Heras et al. (2016). These shrubs are also thought to further facilitate their own encroachment through positive feedbacks (Grover and Musick, 1990; D’Odorico et al., 2012) by modifying their environment in ways that favor continued growth and recruitment, including changes to the local micro-climate (D’Odorico et al., 2010) and rates of soil erosion (Turnbull et al., 2010). Such positive feedback also involve suppression of herbaceous competitors, reducing competition as well as the amount of flammable biomass used to fuel the fires that keep creosotebush growth in check (Van Auken, 2000). We hypothesized that, given potential for positive feedback mechanisms, the rarity of conspecifics at the low-density encroachment front may depress demographic performance and generate pushed-wave dynamics.

104 We used a combination of observational and experimental data from shrub ecotones
 105 in central New Mexico to parameterize a spatial integral projection model (SIPM) that
 106 predicts that speed of encroachment (m/yr) resulting from lower-level demographic and
 107 dispersal processes. Our data came from demographic surveys and experimental trans-
 108 plants along replicate ecotone transects spanning a gradient of shrub density, and seed
 109 drop experiments to estimate the properties of the dispersal kernel. We focused on wind
 110 dispersal of seeds, since little is known about the natural history of dispersal in this
 111 system and the seeds lack rewards to attract animal dispersers. We also used re-surveys
 112 of permanents transects as an independent measure of encroachment that provided a
 113 benchmark against which to evaluate model predictions. The SIPM accounts for size-
 114 structured demography of creosotebush, allows us to test whether shrub expansion is
 115 pulled by the low-density front or pushed from the high-density core, and identifies the
 116 local (demographic) and spatial (seed dispersal) life cycle transitions that most strongly
 117 contribute to expansion speed². We address the following specific questions:

- 118 1. What is the nature of conspecific density dependence in demographic vital rates
 119 along shrub encroachment ecotones? Is encroachment pulled by the individuals at
 120 the front or pushed by individuals behind it?
- 121 2. What is the seed dispersal kernel for this species and how does this vary with
 122 maternal plant size?
- 123 3. What is the predicted rate of expansion from the SIPM and which lower-level
 124 processes most strongly affect the expansion speed?
- 125 4. How does the observed rate of encroachment in the recent past compare to model
 126 predictions?

²*we will need to stay consistent with the language of encroachment/expansion/invasion. For now I am swictihg a lot.*

127 **Materials and methods**

128 **Study species**

129 Creosotebush *Larrea tridentata* is a perennial, drought-resistant shrub that is native to
130 the arid and semiarid regions of the southwestern United States and northern Mexico.
131 High-density areas of creosotebush consist largely of barren soil between plants due to
132 the “islands of fertility” these shrubs create around themselves (Schlesinger et al., 1996;
133 Reynolds et al., 1999), though lower-density areas will often contain grasses in the inter-
134 shrub spaces (Fig. 1). In our northern Chihuahuan desert study region creosotebush
135 reproduces sexually, with numerous small yellow flowers giving rise to highly pubescent
136 spherical fruits several millimetres in diameter; these fruits consist of five carpels, each
137 of which contains a single seed. Seeds are dispersed from the parent plant by gravity and
138 wind, with the possibility for seeds to subsequently be transported by animals or water
139 (Maddox and Carlquist, 1985). In other regions, this species also reproduces asexually
140 and can give rise to long-lived clonal stands (Vasek, 1980), but this does not occur in our
141 study region. The foliage is dark green, resinous, and unpalatable to most grazing and
142 browsing animals (Mabry et al., 1978).

143 **Study site**

144 We conducted our work at the Sevilleta National Wildlife Refuge (SNWR), a Long-Term
145 Ecological Research (SEV-LTER) site in central New Mexico. The refuge exists at the in-
146 tersection of several eco-regions, including the northern Chihuahuan Desert, Great Plains
147 grassland, and steppes of the Colorado Plateau. Annual precipitation is approximately
148 250 mm, with the majority falling during the summer monsoon season from June to
149 September. The recruitment events that facilitate creosotebush expansion are thought
150 to be highly episodic (Peters and Yao, 2012), and this may be linked to fluctuations in
151 monsoon precipitation (Boyd and Brum, 1983; Bowers et al., 2004). Monsoon precipita-

tion during the study years (2013-2017) was [summarise climate data].

Demographic data

Ecotone transects

We collected demographic data during early June of every year from 2013-2017. This work was conducted at **four sites in the eastern part of SNWR**³ (one site was initiated in 2013 and the other three in 2014), with three transects at each site. All transects were situated along a shrubland-grassland ecotone so that a full range of shrub densities was captured: each transect spanned core shrub areas, grassland with no or few shrubs, and the transition between them. Lengths of these transects varied from 200 to 600 m, determined by the strength of vegetation transition since “steep” transitions required less length to capture the full range of shrub density.

We quantified shrub density in 5-meter “windows” along each transect, including all shrubs within one meter of the transect on either side (shrubs that partially overlapped with the census area were included). Densities were quantified once for each transect (in 2013 or 2014) and were assumed to remain constant for the duration of the study, a reasonable assumption for a species with very low recruitment and very high survival of established plants. Given the population’s size structure, we weighted the density of each window by the sizes of the plants, which we quantified as volume (cm³). Volume was calculated as that of an elliptic cone: $V_i = \frac{\pi h}{3} \frac{lw}{4}$ where l , w , and h are the maximum length, maximum width, and height, respectively. Maximum length and width were measured so that they were always perpendicular to each other, and height was measured from the base of the woody stem at the soil surface to the tallest part of the shrub. The weighted density for a window was then expressed as log(volume) summed over all plants in the window.

³*would a map be helpful?*

176 **Observational census**

177 At approximately 50-m intervals along each transect we tagged up to 10 plants for an-
178 nual demographic census and recorded their local (5-m resolution) window so that we
179 could connect individual demographic performance to local density. These tagged shrubs
180 were revisited every June and censused for survival (alive/dead), size (width, length, and
181 height, as above), flowering status, and fertility of flowering plants (numbers of flower-
182 buds, flowers, and fruits). In instances where shrubs had large numbers of reproductive
183 structures that would be difficult to reliably count (a large shrub may have thousands
184 of flowers or fruits), we made counts on a fraction of the shrub and extrapolated to es-
185 timate whole-plant reproduction. Creosotebush does not have one discrete reproductive
186 event per year; instead, flowering may occur throughout much of the warm season. By
187 combining counts of buds, flowers, and fruits we intended to capture a majority of the
188 season's reproductive output, assuming that all buds and flowers will eventually become
189 fruits. Our measurements of reproductive output are therefore conservative and may un-
190 derestimate total seed production for an entire transition year. Each year, we searched
191 for new recruits within one m on either side of the transect. New recruits were tagged
192 and added to the demographic census. The observational census included a total of 522
193 unique individuals.

194 **Transplant experiment**

195 We conducted a transplant experiment in 2015 to test how shrub density affects seedling
196 survival. This approach complemented observational estimates of density dependence
197 and filled in gaps for a part of the shrub life cycle that was rarely observed due to low
198 recruitment. Seeds for the experiment were collected from plants in our study popu-
199 lation in 2014. Seeds were germinated on Pro-Mix potting soil (Quakertown, PA) in
200 Fall 2014 and seedlings were transferred to 3.8 cm-by-12.7 cm cylindrical containers and
201 maintained in a greenhouse at Rice University. Seedlings were transported to SNWR

202 and transplanted into the experiment during July 27-31, 2015. Transplant timing was
203 intended to coincide with the monsoon season, when most natural recruitment occurs.

204 The transplant experiment was conducted at the same four sites and three transects
205 per site as the observational demographic census, where we knew weight shrub densities
206 at 5-m window resolution. We established 12 1-m by 1-m plots along each transect.
207 Plots were intentionally placed to capture density variation: four plots were in windows
208 with zero shrubs, four plots were placed in the top four highest-density windows on the
209 transect, and the remaining four plots were randomly distributed among the remaining
210 windows with weighted density greater than zero. Plots were placed in the middle of
211 each 5-m window (at meter 2.5) and were divided into four 0.5-m by 0.5-m subplots. We
212 divided each subplot into nine squares (0.125-m by 0.125-m) and recorded ground cover
213 of each square as one of the following categories: bare ground, creosotebush, black grama
214 (*B. eriopoda*), blue grama (*B. gracilis*), other grass, or “other”. Each subplot received one
215 transplanted shrub seedling, for a total of 48 transplants per transect, 144 transplants
216 per site, and 576 transplants in the entire experiment. Each site was set up on a different
217 day and there was a significant monsoon event after the third and before the fourth
218 site. This resulted in differential mortality that appears to be related to site (captured
219 as a statistical random effect) but more likely reflects the timing of the monsoon event
220 relative to planting (moist soil likely promoted transplant survival). We revisited the
221 transplant experiment on October 24, 2015 to survey mortality. After that first visit,
222 transplants were censused along with the naturally occurring plants each June, following
223 the methods described above.

224 **Demographic analysis**

225 We fit statistical models to the demographic data and used AIC-based model selection to
226 evaluate empirical support for alternative candidate models. The top statistical models
227 were then used as the vital rate sub-models of the SIPM, so there is a strong connection

228 between the statistical and population modeling, as is typical of integral projection mod-
229 eling. Our analyses focused on the following demographic vital rates: survival, growth,
230 probability of flowering, fertility (flower and fruit production), seedling recruitment, and
231 seedling size. Most of these vital rates were modeled as a function of plant size, and all
232 of them included the possibility of density dependence.

233 The alternative hypotheses of pushed versus pulled wave expansion rest on how the
234 rate of population increase (λ), derived from the combination of all vital rates, respond
235 to density. We were particularly interested in whether demographic performance was
236 maximized as local density goes to zero (pulled) or at non-zero densities behind the
237 wave front (pushed). To flexibly model density dependence and detect non-monotonic
238 responses, we used generalized additive models in the R package ‘mgcv’ (Wood, 2017).
239 For each vital rate, we fit candidate models with or without a smooth term for local
240 weighted density (among other possible covariates). To avoid over-fitting, we set the
241 ‘gamma’ argument of `gam()` to 1.8, which increases the complexity penalty, results in
242 smoother fits (Wood, 2017), and makes our approach more conservative (other gamma
243 values yielded qualitatively similar results). We pooled data across transition years for
244 analysis. All models included the random effect of transect (12 transects across 4 sites);
245 we did not attempt to model both site and transect-within-site random effects due to the
246 low numbers of each. All vital rate functions used the natural logarithm of volume (cm^3)
247 as the size variable and the sum of $\log(\text{volume})$ as the weighted density of a transect
248 window.

249 **Survival** We modeled survival or mortality in year $t+1$ as a Bernoulli random variable
250 with three candidate models for survival probability. These included smooth terms for
251 initial size in year t only (1), initial size and weighted density (2), and both smooth terms
252 plus an interaction between initial size and weighted density (3). We analyzed survival of
253 experimental transplants and observational census plants together in the same analyses,

with a fixed effect of transplant status (yes/no) included in all candidate models. Since recruits and thus mortality events were both very rare in the observational survey, this approach allowed us to “borrow strength” over both data sets to generate a predictive function for size- and possibly density-dependent survival while statistically accounting for differences between experimental and naturally occurring plants. Because we had additional, finer-grained cover data for the transplant experiment that we did not have for the observational census, we conducted an additional stand-alone analysis of transplant survival that explored the influence of covariates at multiple spatial scales (Appendix).

Growth We modeled size in year $t + 1$ as a Gaussian random variable. There were nine candidate models for growth. The simplest model (1) defined the mean of size in year $t + 1$ as a smooth function of size in year t and constant variance. Models (2) and (3) had constant variance but the mean included smooth terms for initial size and weighted density (2) or both smooth terms plus an interaction between initial size and weighted density (3). Models 4-6 had the same mean structure as 1-3 but defined the standard deviation of size in year $t + 1$ as a smooth function of initial size. Models 7-9 mirrored 4-6 and additionally included a smooth term for weighted density in the standard deviation. Modeling growth correctly is important because it defines the probability of any future size conditional on current size, a critical element of the IPM transition kernel. We verified that the AIC-selected model described the data well by simulating data from it and comparing the moments (mean, variance, skewness, and kurtosis) of simulated and real data.

Flowering and fruit production We modeled shrub reproductive status (vegetative or flowering) in year t as a Bernoulli random variable with three candidate models for flowering probability. These included smooth terms for current size (in year t) only (1), size and weighted density (3), and both smooth terms plus an interaction between size and weighted density. We modeled the reproductive output of flowering plants (the sum

280 of flowerbuds, open flowers, and fruits) in year t as a negative binomial random variable.
281 There were three candidate models for mean reproductive output that corresponded to
282 the same three candidates for flowering probability.

283 **Recruitment and recruit size** We modeled seedling recruitment in each transect
284 window as a binomial random variable given the number of total seeds produced in that
285 window in the preceding year. There were two candidate models, with and without
286 an influence of weighted density on the per-seed recruitment probability. To estimate
287 window-level seed production, we used the best-fit models for flowering and fruit produc-
288 tion and applied this to all plants in each window that we observed in our initial density
289 surveys. We assume that recruits come from the previous year's seeds and not from a
290 long-lived soil seed bank.

291 We modeled recruit size as a Gaussian-distributed random variable and fit four can-
292 didate models including an influence of weighted density on mean, variance, both, and
293 neither.

294 **Density-dependent IPM**

295 The size- and density-dependent statistical models comprised the sub-models of a density
296 dependent Integral Projection Model (IPM) that we used to evaluate how the shrub
297 population growth rate responded to con-specific density; we present this non-spatial
298 model before layering on the spatial dynamics generated by seed dispersal. A basic
299 density-independent IPM predicts the number of individuals of size x' at time $t + 1$
300 ($n(x', t + 1)$) based on a projection kernel (K) that gives the rates of transition from
301 sizes x to x' from times t to $t + 1$ and is integrated over the size distribution from the
302 minimum (L) to maximum (U) sizes. In a density-dependent IPM, components of the

303 projection kernel may respond to population abundance and structure:

$$304 \quad n(x', t + 1) = \int_L^U K(x', x, \tilde{n}(t)) n(x, t) dx \quad (1)$$

305 Here, $\tilde{n}(t)$ is some function of population structure $n(x, t)$ such as the total density
 306 of conspecifics ($\tilde{n}(t) = \int n(x, t) dx$) or, as in our case, total density weighted by size
 307 ($\tilde{n}(t) = \int x n(x, t) dx$). For simplicity, in the analyses that follow we do not model density
 308 as a dynamic state variable; instead, we treat density as a static covariate ($\tilde{n}(t) = \tilde{n}$) and
 309 evaluate the IPM at a range of density values. As in our statistical modeling, the size
 310 variable of the IPM (x, x') was $\log(\text{cm}^3)$.

311 For our model, the size- and density-dependent demographic transitions captured by
 312 the projection kernel include growth or shrinkage (g) from size x to x' conditioned on
 313 survival (s) at size x (combined growth-survival function $G(x', x, \tilde{n}) = g(x', x, \tilde{n})s(x, \tilde{n})$),
 314 and the production of new size- x' individuals from size- x parents ($Q(x', x, \tilde{n})$). Repro-
 315 duction reflects the probability of flowering at size x (p), the number of seeds produced
 316 by flowering plants (d), the per-seed probability of recruitment (r), and the size distri-
 317 bution of recruits (c). Collectively, the rate at which x -sized individuals produce x' -sized
 318 individuals at density \tilde{n} is given by the combined reproduction-recruitment function
 319 $Q(x', x, \tilde{n}) = p(x, \tilde{n})d(x, \tilde{n})r(\tilde{n})c(x', \tilde{n})$. Thus, we can express the projection kernel as:

$$320 \quad K(x', x, \tilde{n}) = G(x', x, \tilde{n}) + Q(x', x, \tilde{n}) \quad (2)$$

321 For analysis, we evaluated the IPM kernel over a range of local densities from the min-
 322 imum to the maximum of weighted density values from the 5-meter windows ($0 \leq \tilde{n} \leq$
 323 \tilde{n}_{max}). At each density level, we discretized the IPM kernel into a 200×200 approximat-
 324 ing matrix and calculated the asymptotic growth rate $\lambda(\tilde{n})$ as its leading eigenvalue. We
 325 extended the lower (L) and upper (U) integration limits to avoid unintentional “eviction”
 326 using the floor-and-ceiling method (Williams et al., 2012).

327 We sought to characterize the shape of density dependence: whether fitness declined
 328 monotonically or not with increasing density. We quantified uncertainty in the density-
 329 dependent growth rate $\lambda(\tilde{n})$ by bootstrapping our data. For each bootstrap, we randomly
 330 sampled 75% of our demographic data, re-ran the statistical modeling and model selec-
 331 tion, and used the top vital rate models to generate $\lambda(\tilde{n})$ for that data subset. We
 332 repeated this procedure for 500 bootstrap replicates.

333 **Dispersal modelling**

334 **WALD dispersal model** Dispersal kernels were calculated using the WALD, or Wald
 335 analytical long-distance dispersal, model that uses a mechanistic approach to predict
 336 dispersal patterns of plant propagules by wind. The WALD model, which is based in fluid
 337 dynamics, can serve as a good approximation of empirically-determined dispersal kernels
 338 (Katul et al., 2005; Skarpaas and Shea, 2007) and may be used when direct observations
 339 of dispersal are not available. Under the assumptions that wind turbulence is low, wind
 340 flow is vertically homogenous, and terminal velocity is achieved immediately upon seed
 341 release, the WALD model simplifies a Lagrangian stochastic model to create a dispersal
 342 kernel that estimates the likelihood a propagule will travel a given distance (Katul et al.,
 343 2005). Our dispersal kernel takes the form of the inverse Gaussian distribution

$$344 \quad p(r) = \left(\frac{\lambda'}{2\pi r^3} \right)^{\frac{1}{2}} \exp \left[-\frac{\lambda'(r - \mu')^2}{2\mu'^2 r} \right] \quad (3)$$

345 that is a **slight adaptation**⁴ from equation 5b in Katul et al. (2005), using r to denote
 346 dispersal distance. Here, λ' is the location parameter and μ' is the scale parameter, which
 347 depend on environmental and plant-specific properties of the study system. (We use λ'
 348 for consistency with notation in related papers, but λ' the dispersal location parameter
 349 should not be confused with λ the geometric growth rate.) The location and scale
 350 parameters are defined as $\lambda' = (H/\sigma)^2$ and $\mu' = HU/F$; these are functions of the height

⁴*unclear what this refers to*

351 H of seed release, wind speed U at seed release height, seed terminal velocity F , and
 352 the turbulent flow parameter σ that depends on both wind speed and local vegetation
 353 roughness. We parameterized the WALD dispersal kernel using windspeed data from
 354 the SEV-LTER weather station nearest our study site (Moore and Hall, 2022) and seed
 355 terminal velocity data from laboratory-based seed-drop experiments. Methods for our
 356 seed data collection and technical details of dispersal kernel modeling are provided in
 357 Appendix A.

358 **Spatial integral projection model**

359 We used a spatial integral projection model to piece together seed dispersal and density-
 360 dependent demography, and generate predictions for the rate of shrub expansion that
 361 results from this combination of local and spatial processes. The spatially explicit model
 362 builds upon the non-spatial model (Eq. 1) and adds a spatial variable (z, z') such
 363 that demographic transitions occur across both time and space according to a combined
 364 demography-dispersal kernel \tilde{K} :

$$365 \quad n(x', z', t + 1) = \int_{-\infty}^{+\infty} \int_L^U \tilde{K}(x', x, z', z, \tilde{n}(z, t)) n(x, z, t) dx dz \quad (4)$$

366 Here, $\tilde{K}(x', x, z', z, \tilde{n}(z, t))$ is the rate of transition from size x and location z to size x'
 367 and location z' given density $\tilde{n}(z, t)$ at location z . As before, \tilde{n} is a function of pop-
 368 ulation structure – in our model, weighted local density – but here integrated over an
 369 explicit competitive “neighborhood”: $\tilde{n}(z, t) = \int_{z-h}^{z+h} \int_L^U x n(x, z, t) dx dz$ where h repre-
 370 sents neighborhood size in the units of z .

371 Given that the shrub population at this site is approximately homogeneous perpen-
 372 dicular to the direction of encroachment, expansion is modelled as a wave moving in one
 373 dimension. A spatial integral projection model (SIPM) is used to estimate the speed at
 374 which encroachment occurs; such a model incorporates the effects of variation in traits

like plant size that stage-structured models, such as those described in Neubert and Caswell (2000), do not capture. According to Jongejans et al. (2011), a general SIPM can be formulated as

$$\mathbf{n}(x_2, z_2, t + 1) = \iint \tilde{K}(x_2, x_1, z_2, z_1) \mathbf{n}(x_1, z_1, t) dx_1 dz_1 \quad (5)$$

where x_1 and x_2 are locations of individuals of a particular size before and after one unit of time, and z_1 and z_2 are the respective sizes. The vector \mathbf{n} indicates the population density of each size, and \tilde{K} is a kernel that combines dispersal with demography. Though this SIPM represents a continuous spectrum of shrub sizes and densities, it was implemented by discretising the above integral with a 200 x 200 matrix, as this makes calculations significantly more tractable.

Movement of the wave is determined by the components of the combined dispersal/demography kernel \tilde{K} , which is of the same form as that used in Jongejans et al. (2011). Here,

$$\tilde{K}(x_2, x_1, z_2, z_1) = K(x_2 - x_1)Q(z_2 - z_1) + \delta(x_2 - x_1)G(z_2 - z_1) \quad (6)$$

and K is the dispersal kernel, Q a reproduction function, G a growth function, and δ the Dirac delta function. G is derived from the model for annual growth ratio, and Q is derived from the reproductive structures model as well as other factors including number of seeds per reproductive structure, probability of recruitment from seed, and recruit size. Both G and Q give the probability of transition between sizes; in the case of G , this is the probability of growing from one specific size to another, and in the case of Q the probability that an individual of a specific size produces a recruit of a specific size. The product of K and Q represents the production and dispersal of motile propagules, while the product of G and δ represents the growth of sessile individuals.

Assuming strictly negative density dependence (i.e., pulled waves), the speed of the

399 moving wave can be calculated as

$$400 \quad c^* = \min_{s>0} \left[\frac{1}{s} \ln(\rho_s) \right] \quad (7)$$

401 where s is the wave shape parameter and ρ_s is the dominant eigenvalue of the kernel \mathbf{H}_s
 402 (Jongejans et al., 2011). The kernel \mathbf{H}_s is defined as

$$403 \quad \mathbf{H}_s = M(s)Q(z_2 - z_1) + G(z_2 - z_1) \quad (8)$$

404 where $M(s)$ is the moment-generating function of the dispersal kernel (Jongejans et al.,
 405 2011). For one-dimensional dispersal, this moment-generating function can be estimated
 406 as

$$407 \quad M(s) = \frac{1}{N} \sum_{i=1}^n I_0(sr_i) \quad (9)$$

408 where r is the dispersal distance for each observation, and I_0 is the modified Bessel
 409 function of the first kind and zeroth order (Skarpaas and Shea, 2007). In order to obtain
 410 M , numerous dispersal distances were simulated from the dispersal kernel $K(r)$ described
 411 in the previous section, with over 2000 replications for each shrub height increment of 1
 412 cm. This was performed over the range from the lowest possible dispersal height to the
 413 maximum shrub height. Once $M(s)$ was obtained for dispersal at each shrub height, \mathbf{H}_s
 414 and c^* were calculated for each value of s ; this was done for values of s ranging from 0
 415 to 2, as it is this range in which c^* occurs.

416 Estimates of the wavespeed were bootstrapped for a total of 1000 replicates. Each
 417 bootstrap replicate recreated size- and density-dependent demographic models using 80%
 418 resampling on the original demographic data, and recreated dispersal kernels also using
 419 80% resampling on the wind speeds and seed terminal velocities. Between replicates,
 420 the structure of the demographic models was kept constant, though coefficient estimates
 421 were not; this approach, while effectively ignoring model uncertainty, has the benefit of

422 increasing computational efficiency, which is especially useful given the time-consuming
423 nature of numerically estimating the many dispersal kernels used in the model.

424 **Encroachment re-surveys**

425 We recorded shrub percent cover along two permanent 1000-m transects that spanned
426 the shrub-grass ecotone, from high to low to near-zero shrub density. These surveys were
427 conducted in summer 2001 and again in summer 2013 to document change in creosotebush
428 abundance and spatial extent. At every 10 meters, shrub cover was recorded in nine cover
429 classes (<1%, 1–4%, 5–10%, 10–25%, 25–33%, 33–50%, 50–75%, 75–95%, >95%). For
430 visualization, we show midpoint values of these cover classes at each meter location for
431 both transects and years.

432 **Results**

433 **Size and density dependent demography**

434 Demographic data from naturally occurring and transplanted individuals revealed strong
435 size- and density-dependence in demographic vital rates. For most sizes and vital rates,
436 local density had negative demographic effects. Statistical support for size- and density-
437 dependence is provided in Table XX, which provides AIC rankings for candidate models
438 based on the completed (not bootstrapped) data set.

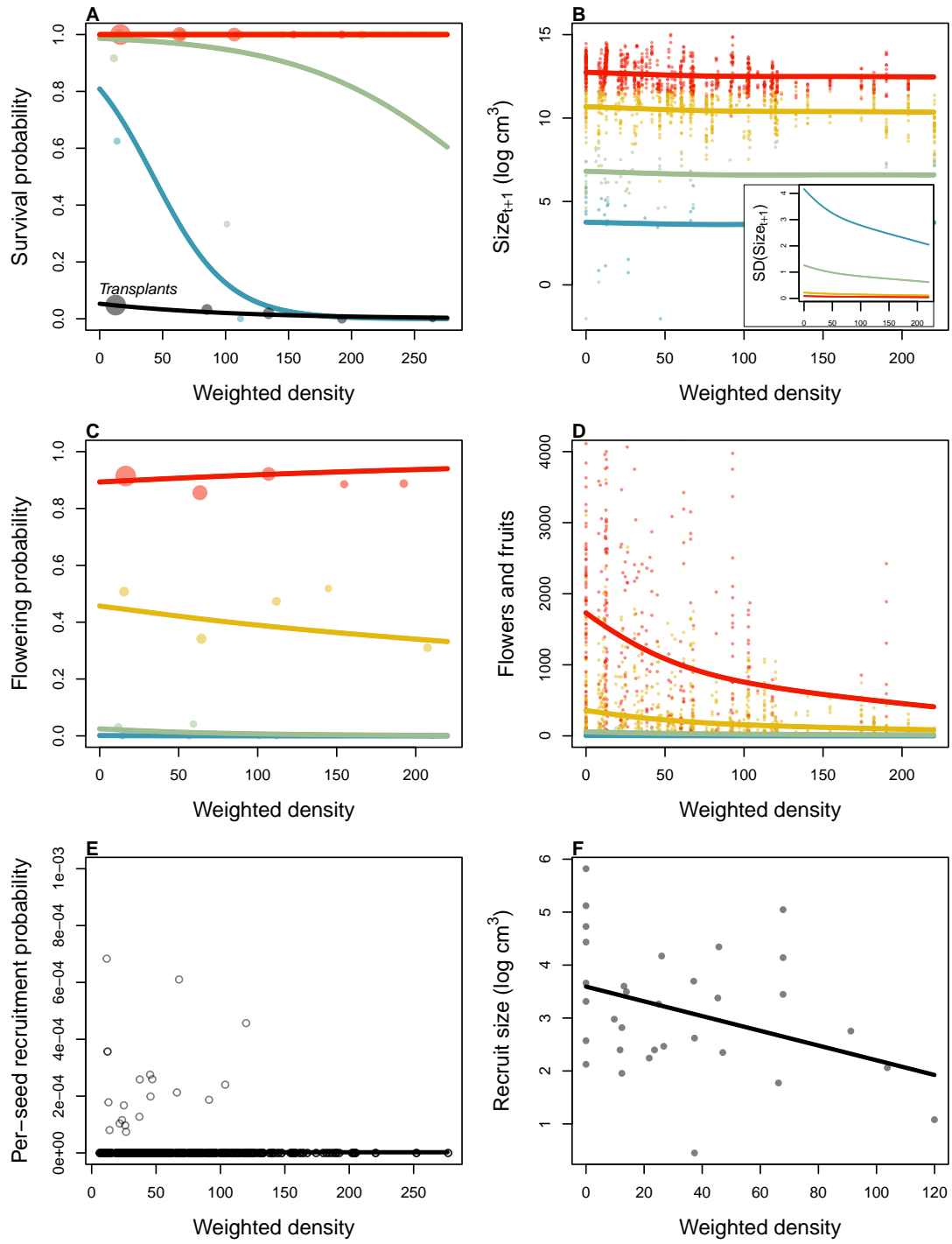


Figure 2: Size- and density-dependence in demographic vital rates. **A** Probability of survival from natural population census and transplant experiment (black line), **B** Mean and variance (inset) of size conditional on previous size, **C** Probability of flowering, **D** Flower and fruit production, **E** Probability of recruitment per seed, **F** Recruit size. In **A–E**, colored lines indicate four size groups (red is largest, blue is smallest), discretized for data visualization only. In all panel, weighted density is the sum of all plant sizes $\log(\text{cm}^3)$ within the same 5-m window as the census individual.

439 **Survival** Among naturally occurring plants, survival of large, established individuals
440 was very high (Fig. 2A). We observed relatively few mortality events and nearly all of
441 these were among new recruits. The probability of survival at these small sizes declined
442 with increasing density. Survival of transplants was very low, lower even than survival
443 of similarly-sized, naturally occurring recruits (Fig. 2B). However, the transplant results
444 support the general pattern of negative density dependence in survival. Among the 20
445 survivors, 15 of them occurred in transect windows below the median of weighted shrub
446 density.

447 SHORT PARAGRAPH SUMMARIZING SMALLER-SCALE ANALYSIS IN AP-
448 PENDIX.

449 **Growth** Current size was strongly predictive of future size, as expected, and there
450 was weak negative density dependence in mean future size conditioned on current size
451 (Fig. 2C). However, there was a stronger signal of density dependence in the variance of
452 future size (Fig. 2C, inset). Plants at low density exhibited greater variance in growth
453 trajectories and this was especially true at the smallest sizes. Thus, large increases in
454 the size of new recruits were most likely to occur under low-density conditions.

455 **Flowering and fruit production** Flowering probability was strongly size-dependent
456 and and very weakly sensitive to local density (Fig. 2D). However, fertility of flowering
457 plants was strongly negative density dependent, with greatest flower and fruit production
458 by the largest plants at the lowest densities, and vice versa (Fig. 2E).

459 **Recruitment and recruit size** We observed 32 natural recruitment events along our
460 transects during the study years and our estimate recruitment rate, given total expected
461 seed production in each window preceding the recruitment year, was very low (2.47×10^{-6} ,
462 2F). While most recruitment events occurred at low density, this is also where most seed
463 production was concentrated (Fig. 2E) and low-density windows were over-represented

relative to high density. For these reasons we were more likely to observe recruitment events at low density. Controlling for sampling effort and seed production, the statistical models indicated that our data were most consistent with a constant, density-independent recruitment rate (Table XX). However, the mean size of new recruits declined significantly with local density (Fig. 2F).

Population growth rate As expected based on the vital rate results, the asymptotic population growth rate λ declined monotonically with density (Fig. 3). This was true across all bootstrap replicates, indicating high certainty that shrub fitness is maximized at zero density and thus that the expansion wave is “pulled”. Mean growth rate at low density was 3% per year, with bootstrap uncertainty spanning 1–6%. At high density in the core of the expansion wave, population growth rates approached $\lambda = 1$, indicating population stasis driven by near-perfect survival and extremely rare recruitment.

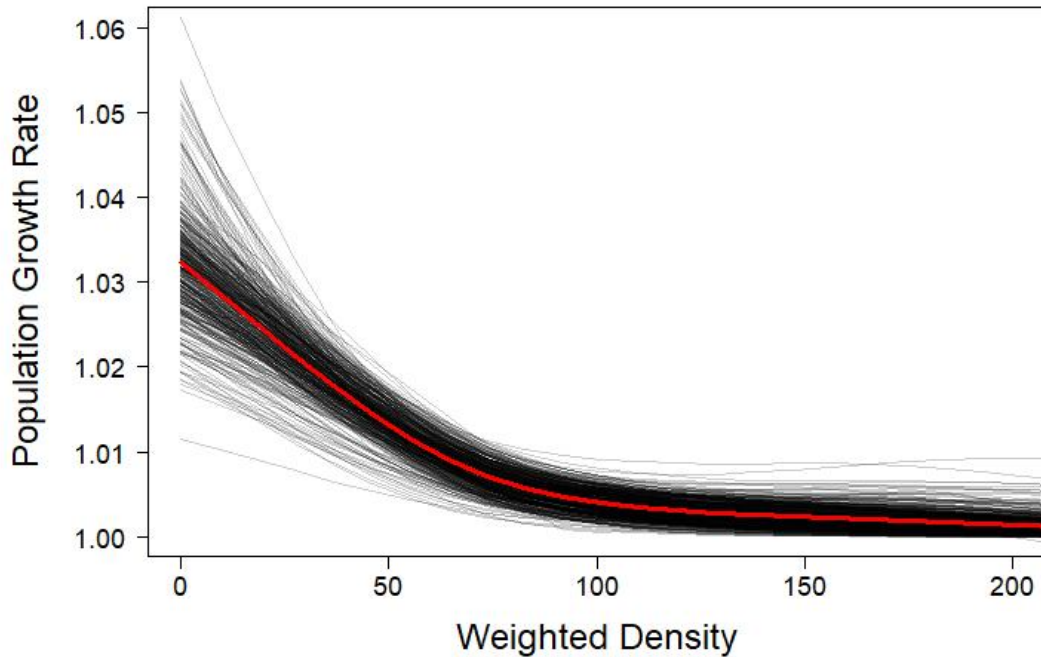


Figure 3: Density dependence in the asymptotic population growth rate (λ). Lines show bootstrap replicates sub-sampled from the full demographic data set. Weighted deighted density is the sum of all plant sizes $\log(cm^3)$ within 5-m windows.

Seed dispersal

As the speed of encroachment is quite limited, so is the extent of wind dispersal. Long distance dispersal events, while more common for taller shrubs than their shorter counterparts, are still uncommon overall. For the tallest shrub height of 1.98 m, only 0.32% of propagules exceed a dispersal distance of 5 m, and 0.02% exceed 10 m. At 1 m, or approximately half the tallest shrub height, long distance dispersal is even less likely, with 0.0046% of propagules exceeding a dispersal distance of 5 m and 0.0009% exceeding 10 m. Given that the median shrub height is only 0.64 m, the occurrence of long-distance wind dispersal in most of the shrub population is highly improbable, and the few instances in which it occurs will only be limited to the tallest shrubs. Thus, as Figure 4 demonstrates,

486 shorter dispersal distances dominate; even for the tallest shrub, 81% of seeds fall within
 487 only a metre of the plant, and this percentage increases as shrub height decreases. Dis-
 488 persal kernels have their highest probability density at dispersal distances between 2 and
 489 8 cm from the shrub; here, as shrub height increases, the most probable dispersal dis-
 490 tance slightly increases while maximum probability density decreases. Regardless of the
 491 shrub height, most dispersal will occur very close to the plant, though increases in shrub
 492 height dramatically increase the likelihood of dispersal at longer distances. It is clear
 493 that the shape of the height-dependent dispersal kernel $K(r)$ varies greatly among the
 494 shrub population given the large range of shrub heights observed; shrubs at lower heights
 495 have more slender kernels with most of the seeds dispersing closer to the plant, while
 496 taller shrubs have kernels with much fatter tails and are more capable of longer-distance
 497 dispersal.

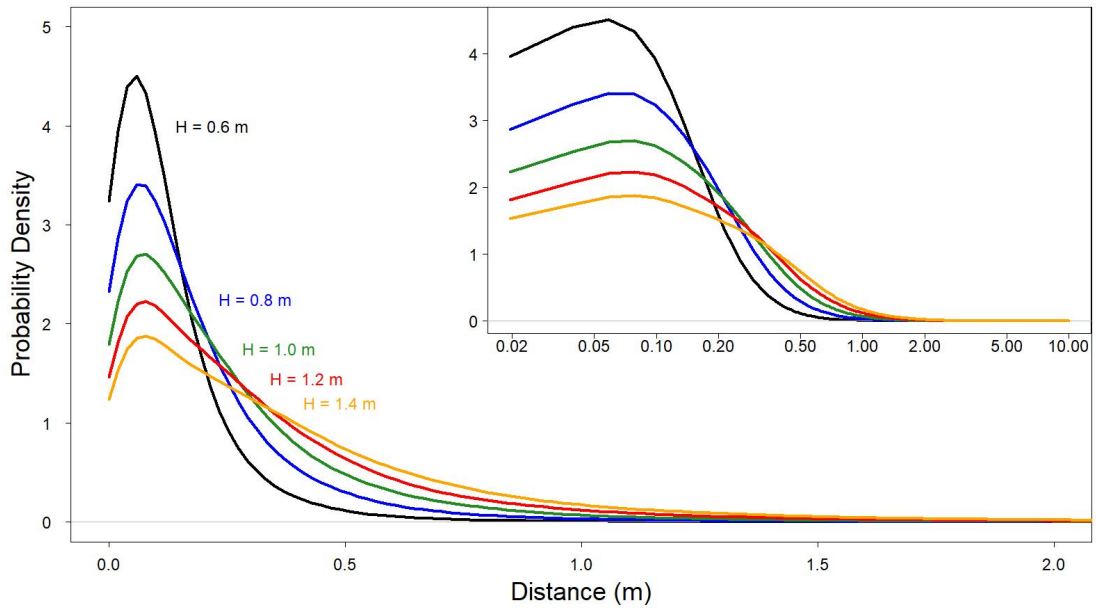


Figure 4: Dispersal kernels, with each colour representing a selected shrub height. The inset plot is the same as the large plot, though with a logarithmic x-axis to more easily show differences in dispersal probability at smaller distances.

Expansion speed

The speed of encroachment at the study site as estimated by the SIPM is rather slow; as can be seen in Figure 5, the low-density wavefront moves at approximately 0.5 cm/yr under normal conditions and at 1 cm/yr under the best seedling survival conditions observed in the dataset. These improved conditions were observed due to above-average rainfall that occurred after greenhouse-grown seedlings were transplanted to the site. Population growth in this low-density region of the moving wave is also low, with a geometric growth rate of $\lambda \approx 1.006$ and even lower rates of growth the higher-density regions behind; in the higher-survival scenario the maximum rate increases to $\lambda \approx 1.013$, with growth still decreasing as density increases. For both scenarios, the decrease in population growth rate with increasing density was monotonic across the range of observed standardised densities, as is shown in Figure 5. This suggests that an Allee effect is likely not present in this population, as the highest rate of population growth is found at the lowest density vanguard of the encroaching population. Thus, the conditions necessary for equation 9 to be valid are satisfied, and these wavespeeds are applicable for a pulled-wave scenario in which no Allee effects are present.

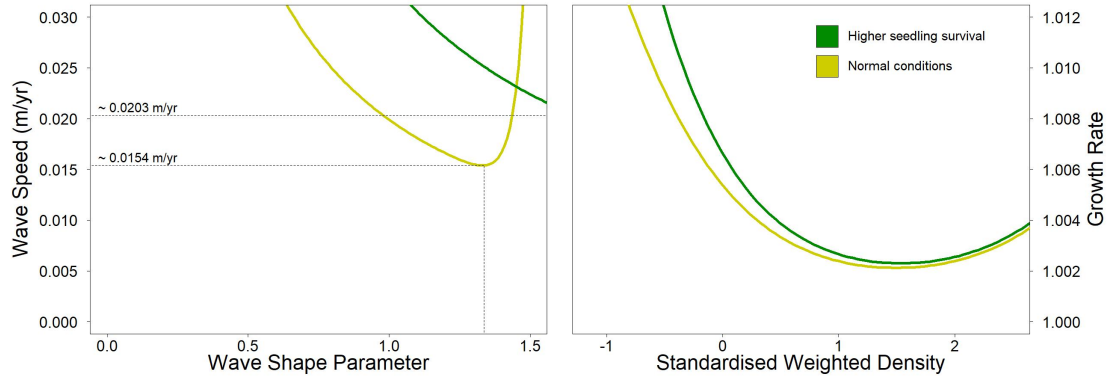


Figure 5: Estimated encroachment wave speeds (left) and geometric rates of population growth (right) for higher post-rainfall seedling survival and normal conditions.

514 Transect re-surveys

515 Re-surveys along two permanent transects revealed virtually no change the in the creosote
 516 expansion wave over 12 years (Fig. 6). There were local changes in percent cover: on
 517 average cover increased by XX% between surveys. However, there was no clear indication
 518 that the leading edge of the creosote shrubland has advanced (the modest right-ward shift
 519 on both transects is within the range of measurement error).

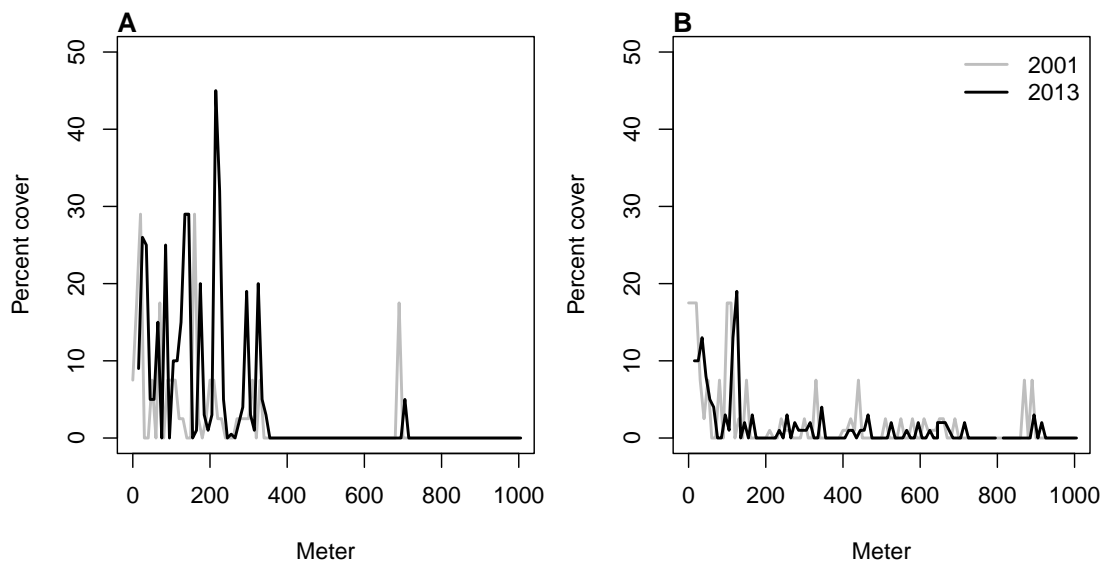


Figure 6: Re-surveys of shrub cover along two permanent trasects (A,B) surveyed in 2001 and 2013.

520 Discussion

521 The slow movement of the encroaching creosotebush wave at the Sevilleta LTER site
 522 can likely be contributed to a combination of three factors: short dispersal distances
 523 with extremely limited long-distance dispersal events, very low probability of recruit-
 524 ment from seed, and high seedling mortality. These three barriers, when combined, form
 525 a formidable challenge to the establishment of new shrubs at the low-density front of
 526 the wave. First, a seed must travel far enough to avoid competition with the parent

527 shrub, which is unlikely given the dispersal kernels shown in Figure 2. Even if the seed
528 manages to be dispersed this far, its chances of becoming a seedling are low. Caching and
529 consumption by seed-eaters such as a variety of seed-harvesting ants (Whitford, 1978;
530 Whitford et al., 1980; Lei, 1999) and the kangaroo rat *Dipodomys merriami* (Chew and
531 Chew, 1970) decreases the amount of seeds available for germination. However, reduc-
532 tion in germination caused by destruction of seeds may be partly mitigated by the more
533 favourable germination conditions that these seeds can experience when cached under-
534 ground (Chew and Chew, 1970). Many of the remaining seeds will still fail to germinate,
535 and in the unlikely event that germination does occur, seedlings will likely die given
536 the high rates of mortality observed in smaller shrubs. Such high rates of creosotebush
537 seedling mortality have been observed in other studies as well (Boyd and Brum, 1983;
538 Bowers et al., 2004), probably due to a combination of herbivory, competition, and abiotic
539 stresses.

540 However, as low as they are, the wavespeed estimates given in this paper are still
541 conservative estimates for reasons mostly related to dispersal. First, it is important to
542 note that the dispersal kernels used here, while they account for variation in factors
543 such as wind speed and terminal velocity, may underestimate the distances that shrub
544 propagules travel. Because the WALD model assumes that terminal velocity is reached
545 immediately upon seed release, seeds in the estimate thus take a shorter time to fall
546 and have less time to be transported by wind, and the true frequency of long-distance
547 dispersal events may thus be greater than what is estimated here. Second, dispersal at the
548 study site could occur through additional mechanisms other than wind. For example,
549 secondary dispersal through runoff from significant rainfall events can transport seeds
550 (Thompson et al., 2014), and given that long-distance dispersal by bird and subsequent
551 species divergence is thought to be responsible for creosotebush being in North America
552 in the first place (Wells and Hunziker, 1976), short-distance dispersal by other animals
553 at the study site likely occurs. As mentioned above, seeds are transported by seed-

554 harvesting ants and granivorous mammals, where they are often stored in caches that
555 can be appreciable distances from the parent shrubs. Whether transportation occurs via
556 ant or rodent, creosotebush seeds can be moved significantly further than wind alone
557 can, though many of these seeds are eventually consumed.

558 Despite the more conservative estimates our model yields, the estimated rate of dis-
559 persal in creosotebush populations at the Sevilleta National Wildlife Refuge is consistent
560 with observations from the past 50-60 years, as creosotebush expansion during this time
561 has been minimal (Moreno-de las Heras et al., 2016). However, it cannot explain the
562 long-term increases in creosotebush cover at the study site, as total encroachment over
563 the past 150 years is much greater than what would be expected given the encroachment
564 rates derived by our models. Such a discrepancy is likely due to much of the expansion
565 occurring in an episodic fashion, with short times during which rapid encroachment oc-
566 curs due to favourable environmental conditions. This could be due in part to seedling
567 recruitment, which is a factor that strongly limits creosotebush expansion, being rare
568 and episodic. For example, Allen et al. (2008) estimate that a major recruitment event
569 occurred at this site in the 1950s, which is supported by photographic evidence from
570 Milne et al. (2003) of a drought-driven expansion during this time. Moreno-de las Heras
571 et al. (2016) estimate that after this expansion, several smaller creosotebush recruitment
572 events occurred in decadal episodes. However, such events can be highly localised and
573 may not necessarily occur at the low-density front of encroachment, which could explain
574 how these recruitment events can still coexist with lack of encroachment in the recent
575 past.

576 Overall, our observations and model highlight three aspects of creosotebush encroach-
577 ment that should be the focus of future studies seeking to obtain better estimates of
578 encroachment rates. First, negative density dependence in survival, growth, and repro-
579 duction is demonstrated, along with size dependence. The clear dependence on size and
580 conspecific density suggests that they both should be considered when estimating cre-

581 osotebush expansion and quantifying the demographic variation that contributes to it.
582 Second, wind dispersal in these shrubs is quite limited; though the dispersal kernels seen
583 here are typical in the sense that they are characterised by high near-plant dispersal and
584 exceptionally low long-distance dispersal, the scale across which such dispersal occurs
585 is small, with most seeds landing within only 1 m of the shrub. Wind dispersal alone
586 may be an underestimate of the true amount of dispersal occurring, and future work
587 should seek to incorporate the effects of dispersal by runoff and animals so that a more
588 representative model of total dispersal can be obtained. Finally, encroachment is slow or
589 even stagnates, but only most of the time. Though our encroachment speed estimates
590 are representative of creosotebush populations for most years, the significant expansion
591 seen over larger time scales suggests that there is episodic expansion in other years; while
592 our model is consistent with the recent stagnation in creosotebush encroachment at the
593 Sevilleta LTER site, a model that also includes interannual variability in factors such
594 as survival and recruitment would be able to better account for instances of episodic
595 population expansion that are characteristic of this location.

596 **Acknowledgements**

597 **Author contributions**

598 **Data accessibility**

599 **References**

- 600 Allen, A., W. Pockman, C. Restrepo, and B. Milne. 2008. Allometry, growth and
601 population regulation of the desert shrub *Larrea tridentata*. *Functional Ecology* pages
602 197–204.
- 603 Bowers, J. E., R. M. Turner, and T. L. Burgess. 2004. Temporal and spatial patterns in

604 emergence and early survival of perennial plants in the Sonoran Desert. *Plant Ecology*
605 **172**:107–119.

606 Boyd, R. S., and G. D. Brum. 1983. Postdispersal reproductive biology of a Mojave Desert
607 population of *Larrea tridentata* (Zygophyllaceae). *American Midland Naturalist* pages
608 25–36.

609 Brandt, J. S., M. A. Haynes, T. Kuemmerle, D. M. Waller, and V. C. Radeloff. 2013.
610 Regime shift on the roof of the world: Alpine meadows converting to shrublands in
611 the southern Himalayas. *Biological Conservation* **158**:116–127.

612 Buffington, L. C., and C. H. Herbel. 1965. Vegetational changes on a semidesert grassland
613 range from 1858 to 1963. *Ecological monographs* **35**:139–164.

614 Bullock, J. M., S. M. White, C. Prudhomme, C. Tansey, R. Perea, and D. A. Hooftman.
615 2012. Modelling spread of British wind-dispersed plants under future wind speeds in
616 a changing climate. *Journal of Ecology* **100**:104–115.

617 Cabral, A., J. De Miguel, A. Rescia, M. Schmitz, and F. Pineda. 2003. Shrub encroach-
618 ment in Argentinean savannas. *Journal of Vegetation Science* **14**:145–152.

619 Chew, R. M., and A. E. Chew. 1970. Energy relationships of the mammals of a desert
620 shrub (*Larrea tridentata*) community. *Ecological Monographs* pages 2–21.

621 D’Odorico, P., J. D. Fuentes, W. T. Pockman, S. L. Collins, Y. He, J. S. Medeiros,
622 S. DeWekker, and M. E. Litvak. 2010. Positive feedback between microclimate and
623 shrub encroachment in the northern Chihuahuan desert. *Ecosphere* **1**:1–11.

624 D’Odorico, P., G. S. Okin, and B. T. Bestelmeyer. 2012. A synthetic review of feedbacks
625 and drivers of shrub encroachment in arid grasslands. *Ecohydrology* **5**:520–530.

626 Gandhi, S. R., E. A. Yurtsev, K. S. Korolev, and J. Gore. 2016. Range expansions
627 transition from pulled to pushed waves as growth becomes more cooperative in an

628 experimental microbial population. *Proceedings of the National Academy of Sciences*
629 **113**:6922–6927.

630 Gardner, J. L. 1951. Vegetation of the creosotebush area of the Rio Grande Valley in
631 New Mexico. *Ecological Monographs* **21**:379–403.

632 Gibbens, R., R. McNeely, K. Havstad, R. Beck, and B. Nolen. 2005. Vegetation changes
633 in the Jornada Basin from 1858 to 1998. *Journal of Arid Environments* **61**:651–668.

634 Goslee, S., K. Havstad, D. Peters, A. Rango, and W. Schlesinger. 2003. High-resolution
635 images reveal rate and pattern of shrub encroachment over six decades in New Mexico,
636 USA. *Journal of Arid Environments* **54**:755–767.

637 Grover, H. D., and H. B. Musick. 1990. Shrubland encroachment in southern New Mexico,
638 USA: an analysis of desertification processes in the American Southwest. *Climatic*
639 *change* **17**:305–330.

640 Hsieh, C.-I., and G. G. Katul. 1997. Dissipation methods, Taylor’s hypothesis, and
641 stability correction functions in the atmospheric surface layer. *Journal of Geophysical*
642 *Research: Atmospheres* **102**:16391–16405.

643 Huang, H., L. D. Anderegg, T. E. Dawson, S. Mote, and P. D’Odorico. 2020. Crit-
644 ical transition to woody plant dominance through microclimate feedbacks in North
645 American coastal ecosystems. *Ecology* **101**:e03107.

646 Jongejans, E., K. Shea, O. Skarpaas, D. Kelly, and S. P. Ellner. 2011. Importance of
647 individual and environmental variation for invasive species spread: a spatial integral
648 projection model. *Ecology* **92**:86–97.

649 Katul, G., A. Porporato, R. Nathan, M. Siqueira, M. Soons, D. Poggi, H. Horn, and
650 S. A. Levin. 2005. Mechanistic analytical models for long-distance seed dispersal by
651 wind. *The American Naturalist* **166**:368–381.

- 652 Keitt, T. H., M. A. Lewis, and R. D. Holt. 2001. Allee effects, invasion pinning, and
653 species' borders. *The American Naturalist* **157**:203–216.
- 654 Kelleway, J. J., K. Cavanaugh, K. Rogers, I. C. Feller, E. Ens, C. Doughty, and N. Sain-
655 tilan. 2017. Review of the ecosystem service implications of mangrove encroachment
656 into salt marshes. *Global Change Biology* **23**:3967–3983.
- 657 Knapp, A. K., J. M. Briggs, S. L. Collins, S. R. Archer, M. S. BRET-HARTE, B. E.
658 Ewers, D. P. Peters, D. R. Young, G. R. Shaver, E. Pendall, et al. 2008. Shrub
659 encroachment in North American grasslands: shifts in growth form dominance rapidly
660 alters control of ecosystem carbon inputs. *Global Change Biology* **14**:615–623.
- 661 Kot, M., M. A. Lewis, and P. van den Driessche. 1996. Dispersal data and the spread of
662 invading organisms. *Ecology* **77**:2027–2042.
- 663 Lei, S. A. 1999. Ecological impacts of *Pogonomyrmex* on woody vegetation of a *Larrea*-
664 *Ambrosia* shrubland. *The Great Basin Naturalist* pages 281–284.
- 665 Lewis, M., and P. Kareiva. 1993. Allee dynamics and the spread of invading organisms.
666 *Theoretical Population Biology* **43**:141–158.
- 667 Mabry, T. J., J. H. Hunziker, D. Difeo Jr, et al. 1978. Creosote bush: biology and
668 chemistry of *Larrea* in New World deserts. Dowden, Hutchinson & Ross, Inc.
- 669 Maddox, J. C., and S. Carlquist. 1985. Wind dispersal in Californian desert plants:
670 experimental studies and conceptual considerations. *Aliso: A Journal of Systematic*
671 *and Evolutionary Botany* **11**:77–96.
- 672 Milne, B. T., D. I. Moore, J. L. Betancourt, J. A. Parks, T. W. Swetnam, R. R. Par-
673 menter, and W. T. Pockman. 2003. Multidecadal drought cycles in south-central New
674 Mexico: Patterns and consequences. Oxford University Press: New York, NY.

- 675 Moore, D., and K. Hall, 2022. Meteorology Data from the Sevilleta
676 National Wildlife Refuge, New Mexico. Environmental Data Initiative.
677 <https://doi.org/10.6073/pasta/d56307b398e28137dabaa6994f0f5f92>.
- 678 Moreno-de las Heras, M., L. Turnbull, and J. Wainwright. 2016. Seed-bank structure
679 and plant-recruitment conditions regulate the dynamics of a grassland-shrubland Chi-
680 huahuan ecotone. *Ecology* **97**:2303–2318.
- 681 Mugasi, S., E. Sabiiti, and B. Tayebwa. 2000. The economic implications of bush
682 encroachment on livestock farming in rangelands of Uganda. *African Journal of Range
683 and Forage Science* **17**:64–69.
- 684 Nathan, R., G. G. Katul, G. Bohrer, A. Kupařinen, M. B. Soons, S. E. Thompson,
685 A. Trakhtenbrot, and H. S. Horn. 2011. Mechanistic models of seed dispersal by wind.
686 *Theoretical Ecology* **4**:113–132.
- 687 Neubert, M. G., and H. Caswell. 2000. Demography and dispersal: calculation and
688 sensitivity analysis of invasion speed for structured populations. *Ecology* **81**:1613–
689 1628.
- 690 Oba, G., E. Post, P. Syvertsen, and N. Stenseth. 2000. Bush cover and range condition
691 assessments in relation to landscape and grazing in southern Ethiopia. *Landscape
692 ecology* **15**:535–546.
- 693 Pan, S., and G. Lin. 2012. Invasion traveling wave solutions of a competitive system
694 with dispersal. *Boundary Value Problems* **2012**:120.
- 695 Parizek, B., C. M. Rostagno, and R. Sottini. 2002. Soil erosion as affected by shrub
696 encroachment in northeastern Patagonia. *Rangeland Ecology & Management/Journal
697 of Range Management Archives* **55**:43–48.

- 698 Peters, D. P., and J. Yao. 2012. Long-term experimental loss of foundation species:
699 consequences for dynamics at ecotones across heterogeneous landscapes. *Ecosphere*
700 **3**:1–23.
- 701 Ratajczak, Z., J. B. Nippert, and S. L. Collins. 2012. Woody encroachment decreases
702 diversity across North American grasslands and savannas. *Ecology* **93**:697–703.
- 703 Raupach, M. 1994. Simplified expressions for vegetation roughness length and zero-
704 plane displacement as functions of canopy height and area index. *Boundary-Layer*
705 *Meteorology* **71**:211–216.
- 706 Ravi, S., P. D’Odorico, S. L. Collins, and T. E. Huxman. 2009. Can biological invasions
707 induce desertification? *The New Phytologist* **181**:512–515.
- 708 Reed, M., L. Stringer, A. Dougill, J. Perkins, J. Athopheng, K. Mulale, and N. Favretto.
709 2015. Reorienting land degradation towards sustainable land management: Linking
710 sustainable livelihoods with ecosystem services in rangeland systems. *Journal of envi-*
711 *ronmental management* **151**:472–485.
- 712 Reynolds, J. F., R. A. Virginia, P. R. Kemp, A. G. De Soyza, and D. C. Tremmel. 1999.
713 Impact of drought on desert shrubs: effects of seasonality and degree of resource island
714 development. *Ecological Monographs* **69**:69–106.
- 715 Roques, K., T. O’connor, and A. R. Watkinson. 2001. Dynamics of shrub encroach-
716 ment in an African savanna: relative influences of fire, herbivory, rainfall and density
717 dependence. *Journal of Applied Ecology* **38**:268–280.
- 718 Schlesinger, W. H., and A. M. Pilmanis. 1998. Plant-soil interactions in deserts. *Biogeo-*
719 *chemistry* **42**:169–187.
- 720 Schlesinger, W. H., J. A. Raikes, A. E. Hartley, and A. F. Cross. 1996. On the spatial

721 pattern of soil nutrients in desert ecosystems: ecological archives E077-002. *Ecology*
722 **77**:364–374.

723 Schlesinger, W. H., J. F. Reynolds, G. L. Cunningham, L. F. Huenneke, W. M. Jarrell,
724 R. A. Virginia, and W. G. Whitford. 1990. Biological feedbacks in global desertification.
725 *Science* **247**:1043–1048.

726 Sirami, C., and A. Monadjem. 2012. Changes in bird communities in Swaziland savannas
727 between 1998 and 2008 owing to shrub encroachment. *Diversity and Distributions*
728 **18**:390–400.

729 Skarpaas, O., and K. Shea. 2007. Dispersal patterns, dispersal mechanisms, and invasion
730 wave speeds for invasive thistles. *The American Naturalist* **170**:421–430.

731 Sullivan, L. L., B. Li, T. E. Miller, M. G. Neubert, and A. K. Shaw. 2017. Density depen-
732 dence in demography and dispersal generates fluctuating invasion speeds. *Proceedings*
733 *of the National Academy of Sciences* **114**:5053–5058.

734 Taylor, C. M., and A. Hastings. 2005. Allee effects in biological invasions. *Ecology*
735 *Letters* **8**:895–908.

736 Thompson, S. E., S. Assouline, L. Chen, A. Trahtenbrot, T. Svoray, and G. G. Katul.
737 2014. Secondary dispersal driven by overland flow in drylands: Review and mechanistic
738 model development. *Movement ecology* **2**:7.

739 Trollope, W., F. Hobson, J. Danckwerts, and J. Van Niekerk. 1989. Encroachment and
740 control of undesirable plants. *Veld management in the Eastern Cape* pages 73–89.

741 Turnbull, L., J. Wainwright, and R. E. Brazier. 2010. Changes in hydrology and erosion
742 over a transition from grassland to shrubland. *Hydrological Processes: An Interna-*
743 *tional Journal* **24**:393–414.

- 744 Van Auken, O. 2009. Causes and consequences of woody plant encroachment into western
745 North American grasslands. *Journal of environmental management* **90**:2931–2942.
- 746 Van Auken, O. W. 2000. Shrub invasions of North American semiarid grasslands. *Annual*
747 *review of ecology and systematics* **31**:197–215.
- 748 Vasek, F. C. 1980. Creosote bush: Long-lived clones in the Mojave Desert. *American*
749 *Journal of Botany* **67**:246–255.
- 750 Veit, R. R., and M. A. Lewis. 1996. Dispersal, population growth, and the Allee ef-
751 fect: dynamics of the house finch invasion of eastern North America. *The American*
752 *Naturalist* **148**:255–274.
- 753 Wang, M.-H., M. Kot, and M. G. Neubert. 2002. Integrodifference equations, Allee
754 effects, and invasions. *Journal of mathematical biology* **44**:150–168.
- 755 Wells, P. V., and J. H. Hunziker. 1976. Origin of the creosote bush (*Larrea*) deserts of
756 southwestern North America. *Annals of the Missouri Botanical Garden* pages 843–861.
- 757 Whitford, W., E. Depree, and P. Johnson. 1980. Foraging ecology of two chihuahuan
758 desert ant species: *Novomessor cockerelli* and *Novomessor albigulosus*. *Insectes Sociaux*
759 **27**:148–156.
- 760 Whitford, W. G. 1978. Structure and seasonal activity of Chihuahua desert ant commu-
761 nities. *Insectes Sociaux* **25**:79–88.
- 762 Wiernga, J. 1993. Representative roughness parameters for homogeneous terrain.
763 *Boundary-Layer Meteorology* **63**:323–363.
- 764 Williams, J. L., T. E. Miller, and S. P. Ellner. 2012. Avoiding unintentional eviction
765 from integral projection models. *Ecology* **93**:2008–2014.
- 766 Wood, S. 2017. *Generalized Additive Models: An Introduction with R*. 2 edition.
767 Chapman and Hall/CRC.

Appendix A: Dispersal kernel modeling

WALD dispersal kernel In order to create the dispersal kernel, we first take the wind speeds at measurement height z_m and correct them to find wind speed U for any height H by using the logarithmic wind profile ⁵

$$U = \frac{1}{H} \int_{d+z_0}^H \frac{u^*}{K} \log \left(\frac{z-d}{z_0} \right) dz \quad (\text{A1})$$

given in Bullock et al. (2012) equation 6, with the notation slightly modified. Here, z is the height above the ground, K is the von Karman constant, and u^* is the friction velocity. The zero-plane displacement d and roughness length z_0 are surface roughness parameters that, for a grass canopy height h above the ground, are approximated by $d \approx 0.7h$ and $z_0 \approx 0.1h$. These estimates are from Raupach (1994) for a canopy area index $\Lambda = 1$ in which the sum of grass canopy elements is equal to the unit area being measured. A 0.15 m grass height at our study site gives $d = 0.105$ and z_0 , which are suitable approximations for grassland (Wiernga, 1993). Calculations of u^* were done using equation A2 from Skarpaas and Shea (2007), in which

$$u^* = KU_m \left[\log \left(\frac{z_m - d}{z_0} \right) \right]^{-1} \quad (\text{A2})$$

and U_m is the mean wind velocity at the measurement height z_m . Values for the turbulent flow parameter σ were then calculated using the estimate made by Skarpaas and Shea (2007) in their equation A4, where

$$\sigma = 2A_w^2 \sqrt{\frac{K(z-d)u^*}{C_0U}} \quad (\text{A3})$$

and C_0 is the Kolmogorov constant. A_w is a constant that relates vertical turbulence to friction velocity and is approximately equal to 1.3 under the assumptions of above-

⁵ *We need to describe and cite the wind data used here.*

canopy flow made by Skarpaas and Shea (2007), based off calculations from Hsieh and Katul (1997). In addition, the assumption that $z = H$ was made in order to make the calculation of σ more feasible.⁶

The values from the previous three equations give us the necessary information to calculate μ' and λ' , thus allowing us to create the WALD distribution $p(r)$. However, the base WALD model does not take into account variation in wind speeds or seed terminal velocities, which limits its applicability in systems where such variation is present. In order to account for this variation, we integrate the WALD model over distributions of these two variables using the same method as Skarpaas and Shea (2007). Additionally, the WALD model assumes seed release from a single point source, which is not realistic for creosote bush; because seeds are released across the entire height of the shrub rather than from a point source, we integrated $p(r)$ across the uniform distribution from the grass canopy height to the shrub height. Thus, under the assumptions that the height at which a seed is located does not affect its probability of being released and that seeds are evenly distributed throughout the shrub, this gives the dispersal kernel $K(r)$, where

$$K(r) = \iiint p(F)p(U)p(z)p(r) dF dU dz \quad (\text{A4})$$

and $p(F)$ and $p(U)$ are the PDFs of the terminal velocity F and wind speed U , respectively, and $p(z)$ is the uniform distribution from h to H .

Dispersal data collection The distribution $p(F)$ in the integral above was constructed using experimentally determined seed terminal velocities. This was done by using laboratory-based seed release experiments with a high-speed camera and motion tracking software to determine position as a function of time. We then used the Levenberg-Marquardt algorithm to solve a quadratic-drag equation of motion for F . Before seeds were released, they were dried, dyed with yellow fluorescent powder, and then

⁶ *Can you describe this assumption in biological terms?*

813 put against a black background to improve visibility and make tracking easier. While the
814 powder added mass to the seeds, this added mass only yielded an approximately 2.5%
815 increase, likely having little effect on terminal velocities. Measurements were conducted
816 for 48 seeds that were randomly chosen from a seed pool derived from different plants,
817 and then an empirical PDF of terminal velocities was constructed using the data. Con-
818 structing $p(U)$ involved creating an empirical PDF of hourly wind speeds using data from
819 a Sevilleta LTER meteorological station (Five Points), the station closest to our transects.
820 We used wind speed data collected from 1988 to 2010.⁷

⁷ *Most SEV data sets have a doi, so ideally we should cite the wind speed data.*

Appendix B: Model selection results

surv	df	dAIC
~size + transplant + size:transplant + (1 transect)	11.50	1.72
~size + transplant + density + size:transplant + density:transplant + (1 transect)	13.19	0.19
~size + transplant + density + size:transplant + density:transplant + size:density + size:transplant:density + (1 transect)	14.22	0.00

Table B1: AIC model selection for survival probability.

mean(size)	sd(size)	df	dAIC
~size + (1 transect)	~1	3.00	1024.88
~size + density + (1 transect)	~1	8.50	977.23
~size + density + size:density + (1 transect)	~1	10.47	975.17
~size + (1 transect)	~size	9.65	146.23
~size + density + (1 transect)	~size	16.24	19.45
~size + density + size:density + (1 transect)	~size	18.55	19.62
~size + (1 transect)	~size + density	10.40	115.52
~size + density + (1 transect)	~size + density	18.97	0.08
~size + density + size:density + (1 transect)	~size + density	21.33	0.00

Table B2: AIC model selection for mean and variance of future size

Pr(Flowering)	df	dAIC
~size + (1 transect)	5.78	0.63
~size + density + (1 transect)	6.80	2.32
~size + density + size:density + (1 transect)	7.24	0.00

Table B3: AIC model selection for flowering probability.

No. fruits	df	dAIC
~size + (1 transect)	14.25	71.99
~size + density + (1 transect)	5.52	0.00
~size + density + size:density + (1 transect)	6.23	0.37

Table B4: AIC model selection for fruit number.

Pr(Recruitment)	df	dAIC
~(1 transect)	6.57	0.00
~density + (1 transect)	7.39	0.93

Table B5: AIC model selection for recruitment probability.

mean(size)	sd(size)	df	dAIC
~(1 transect)	~1	2.00	2.90
~density+(1 transect)	~1	4.42	0.00
~(1 transect)	~density	3.00	4.74
~density+(1 transect)	~density	5.56	1.21

Table B6: AIC model selection for mean and variance of recruit size.